Nanoimprint Lithography for Molecular-Motor-Based Devices

Emelie Haettner

October 25, 2016

Supervisors:

Heiner Linke
Frida Lindberg

Examiner:

Christelle Prinz

Abstract

Nanoimprint lithography (NIL) can be used for large scale fabrication of topologically structured surfaces. Structures with a resolution down to 10 nm can be manufactured. This report describes the NIL fabrication of a type of molecular-motor-based device. These devices have, up to now, been fabricated with electron beam lithography (EBL). By using NIL instead, future mass production of devices would be possible. The device has previously contained both 200 nm wide nanochannels as well as 80 μm wide, open areas, called loading zones. The large size difference is problematic in NIL. Patterns were therefore added to the open space of the loading zones. The designs created in this work were tested in Matlab simulations, performed by a collaborator. By patterning the loading zones it was also possible to control their loading speed. A NIL-compatible polymer resist, TU7, was tested as a material for the device structures. TU7 was shown to also compatible with the molecular motors in the device. A master stamp was used to fabricate an intermediate polymer stamp (IPS) in a NIL-process. The IPS was then used to imprint the structures in TU7, in a second NIL-process. The result of the imprint was successful.

Contents

1 Background

Within our cells there are a group of proteins called molecular motors. Molecular motors are responsible for directed motion inside the cell. They are involved in processes such as shaping the cell membrane, transporting material in cargoes from one part of the cell to another, and transporting material across the cell membrane, as illustrated in Figure 1. [1]

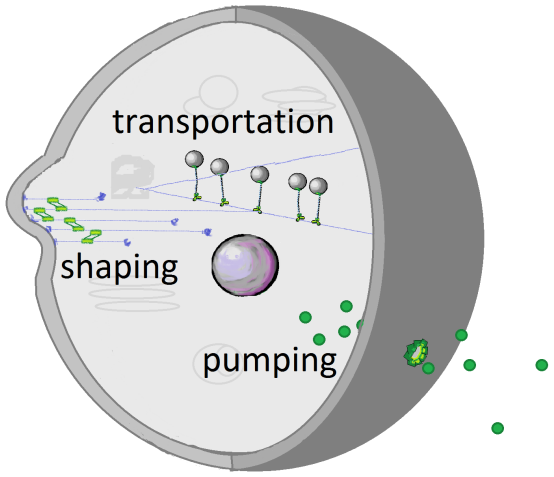

Figure 1: Illustration of different types of molecular motors. Molecular motors can transport material along tracks in the cell and pump across the cell membrane. They are also involved in shaping the cell membrane.

Molecular motors have dimensions on the order of tens of nanometers. They are powered by energy rich compounds, by direct conversion of chemical energy into mechanical work. The generation of heat is therefore small, which make them energy efficient, some of them reaching nearly 100 %. Their small size and energy efficiency make these molecules interesting from an engineering perspective. By integrating them in engineered devices, they can be used to transport and organize molecules at the nanoscale. [2]

Many applications of molecular motors have been suggested. Their ability to transport material has been proposed to be used in for example sensor applications. This could be achieved by letting molecular motors collect analytes from a large sample volume and deliver them to, and locally concentrate them at, a detection point. [3] Another idea that has been suggested, is to pump a microfluidic system. The molecular motors would bind then to microspheres and transport them through a microchannel, pushing liquid in front of them, as described in [4]. A third example,

presented in [5], uses molecular motors to transport synthetic capsules. The capsules can be loaded with several different compounds and are envisioned to be used in, for example, a drug-delivery system.

This report will focus on devices in which biomolecules are transported through a network of nanochannels, by the use of molecular motors. These biomolecules are threadlike proteins, called actin filaments. An example of an application of such a device is a parallel computing machine. Parallel computing, as opposed to serial computing, means that several operations are performed simultaneously. The aim is to be able to find the solution to complex mathematical problems, where the set of possible solutions grow exponentially with the number of included variables, n. A serial computer need exponential time to find the solution, which for large n means that it is practically impossible to do. With parallel computing, the hope is to solve these problems in polynomial time instead. A prototype of this computing device has been presented in [6]. It can perform a simple calculation in a parallel manner with the help of molecular motors.

In order to use molecular motors in devices like the computer, their transportation of actin filaments must be controlled. The molecular motors are therefore immobilized on the floor surfaces of 200 nm wide nanochannels. The nanochannel walls direct the motion, by acting as fences for the transported filaments, as illustrated in Figure 2. [7][8]

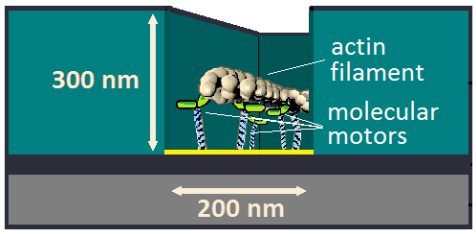

Figure 2: The cross section of a nanochannel for guiding of actin filaments. The channel floor binds to molecular motors. These, in turn, interacts with the filaments by transporting them forward.

Structures called loading zones are used to feed the filaments into the nanochannels, as illustrated in Figure 3 a). The outline of the loading zone wall is drop shaped. Thereby it acts as a funnel which guide filaments to its bottom, where they exit. The loading zone is approximately 80 μm at its widest point. [9]

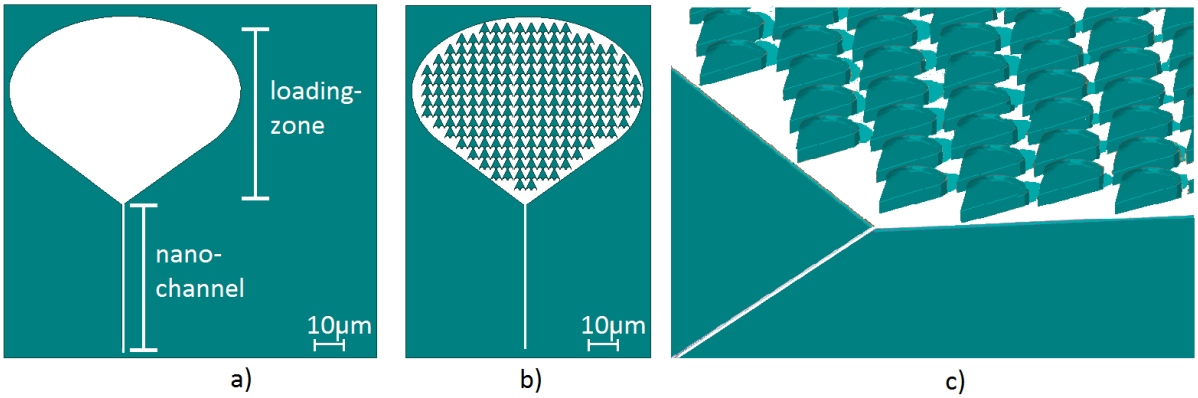

Figure 3: a) Illustration of a loading zone, which feed actin filaments into a nanochannel. b) Illustration of a patterned loading zone. c) Illustration of the topography of a patterned loading zone.

Devices have so far been fabricated with electron beam lithography [6], EBL. EBL uses an electron beam to selectively expose a sample surface. The exposure either cause polymer cross linking or breaking of chemical bonds. Thus, the material solubility is locally changed. This enables patterning of a surface. EBL can achieve a high resolution down to approximately 10 nm. The downside is that EBL is slow and expensive since the structures are individually engraved by the beam one after an other. Therefore, other methods must be used when scaling up production. [10]

Nanoimprint lithography, NIL, is a method of replicating nanostructures with high resolution. A patterned stamp is used to imprint a ductile material, which conforms to the relief. The material is solidified during imprint, after which the stamp can be removed. The whole pattern is fabricated parallelly in one step, which makes it fast. NIL is therefore suitable for mass fabrication.

NIL has been tested for the purpose of imprinting nanochannels for molecular motor transported actin filaments. Straight parallel channels of 100-150 nm depth and of widths ranging from 200-400 nm were imprinted in PMMA on a one inch wafer. [12] However complex patterns, which include both large loading zones as well as nanochannels, have not been fabricated with this method before.

The project was divided into four parts. First, a polymer resist, TU7, which is imprintable with NIL, was tested as material for the walls of the structures. The wall material should not bind molecular motors, to work

as a fence. TU7 turned out to be suitable. Secondly, the loading zone was geometrically redesigned to be imprintable with NIL. Patterns were added to the open area of the loading zones, as shown examples of in Figure 3 b) and c). The patterning brought a possibility of varying the loading rate of actin filaments into the nanochannels. The loading rates of the new loading zones were tested in simulations in Matlab (Till Korten, TU Dresden). In the third step, a master stamp was fabricated. Devices were thereafter imprinted in a two-step NIL process, which included making an intermediate polymer stamp (IPS). The first results showed well imprinted loading zones and nanochannels. As a fourth step, imprinted structures were to be tested in vitro, however this step remains for future work. Further steps include manufacturing large nanochannels networks, that cover wafer surfaces of at least four inches.

2 Theory

2.1 Myosin II

Myosin II is a molecular motor, which is involved in muscle contraction. It is fueled by a compound called adenosine triphosphate (ATP). Figure 4 shows an illustration of myosin II (modified from [9], Mercy Lard 2014). The protein is an intertwined dimer, each monomer containing a globular ATPase head. These heads enable myosin II to bind to filamentous actin, or f-actin. In the presence of ATP, f-actin bound myosin II, starts to move along the filaments. [1]

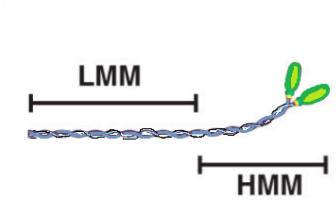

Figure 4: Schematic illustration of myosin II from Figure 2.1 in Ref [9]. The body of myosin II can be divided into light meromyosin (LMM) and heavy meromyosin (HMM).

Myosin II can be separated by enzymatic cleavage into light meromyosin (LMM) and heavy meromyosin (HMM) [13], as indicated in Figure 4. In the computing device described in this report, only the HMM part of myosin II is used.[9]

2.2 Filamentous actin

Actin is a structural protein inside our cells. Actin monomers can organize themselves to form f-actin, consisting of a double helix. F-actin has a diameter of approximately 7nm, while being several micrometers long [1]. It has a persistence length of approximately 10 μm. [14] The filament has two non-identical ends (a plus end and a minus end), causing a structural polarization.[1]

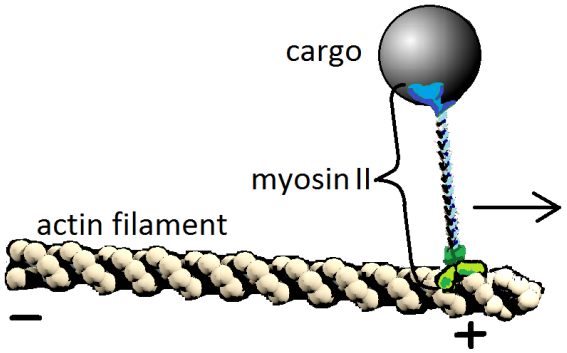

Figure 5: Illustration of myosin II and f-actin. The myosin heads (green) bind to f-actin one head at a time, moving towards the plus end.

Because of the polarization, myosin II can only move along f-actin, in one direction, as illustrated in Figure 5.

2.3 Structure of molecular-motor-based devices for guiding of actin filaments

The molecular-motor-based devices described here, use immobilized HMM to transport f-actin. Thus, f-actin is moving while HMM remains still, and not the other way around as in cells. F-actin and HMM are biomolecules. Therefore the devices need to be immersed in a buffer solution. The structures, including nanochannels and loading zones, are open at the top towards the buffer. The floors and the walls of the structures have a different surface chemistry. It is thereby possible to selectively bind HMM to the floors. Floors are made of SiO_2 which is silanized with trimethylchlorosilane (TMCS). TMCS self-assembles to form a monolayer by creating [Si-O-Si]-bonds to the SiO_2-surface. [17] The TMCS-coating is hydrophobic, which lets HMM to bind with the two functional heads directed towards the buffer. Thus, the heads are free to interact with f-actin. [15]

The walls are made of a polymer resist. The polymer needs to be non-poisonous to the biomolecules. It is also important that HMM do not bind to the polymer in its functional configuration. This is prevented by plasma ashing the device, which makes the polymer hydrophilic. [15] [18] The cross section of a nanochannel structure is illustrated in Figure 6.

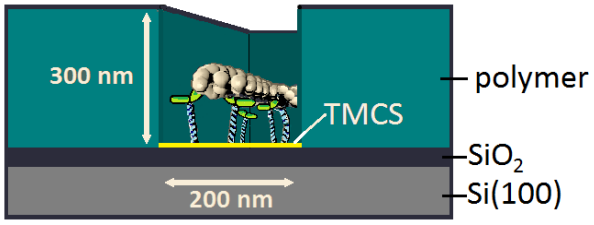

Figure 6: The cross section of an actin guiding nanochannel. The channel floor and walls are made of different materials. The SiO_2-floor is silanized with TMCS which binds to HMM. The two functional heads of HMM is directed towards the buffer, enabling transportation of f-actin.

In order to have a functional device, it has to be ensured that the filaments do not make U-turns. Therefore, the stiffness of f-actin limits the width of the nanochannels. U-turns have previously been observed for f-actin in 500 nm wide channels or more, and an estimated limit for rectifying their motion is between 300-500 nm. Thus the channel width should be less than 300 nm, and is set to 200 nm. The height is set to 300 nm. [15]

The device contains a network of nanochannels. It is important that the crossings and junctions of nanochannels are well resolved to avoid filaments taking non-allowed routes inside the network. A resolution of 10 nm is estimated to be needed to properly guide the filaments in these structures.

Filaments are fed into the nanochannel network by an approximately 80 μm wide, tapered area called a loading zone, which has the same type of walls and HMM-coated floors as the nanochannels. A schematic illustration of a device is shown in Figure 7.

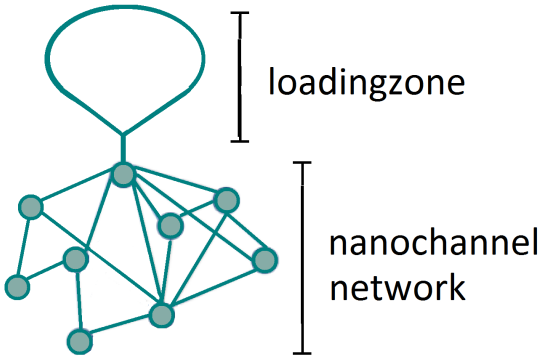

Figure 7: Schematic illustration of a molecular-motor-based device containing a loading zone and a nanochannel network.

The structures described above put up the following requirements of NIL fabrication and imprinting material:

- the SiO_2 surface of the channel floors, needs to be uncovered by the imprinting material
- the imprinting polymer needs to suppress motility by not binding to HMM
- the imprinting polymer needs to be non-poisonous to HMM and f-actin
- crossings of nanochannels require a resolution of approximately 10 nm

2.4 Nanoimprint lithography, NIL

2.4.1 Principle of NIL

Nanoimprint lithography is a method to produce replicas of nanostructures. The basic principle of NIL is illustrated in Figure 8. A stamp is pressed into a ductile polymer, called a resist. The resist is solidified while in contact with the stamp. The stamp can thereafter be removed, leaving a negative copy of the stamp pattern imprinted in the resist. [11] NIL can achieve sub-10 nm resolution. Since NIL is a mechanical process, the resolution of the imprint mainly depends on the resolution of the stamp. [19]

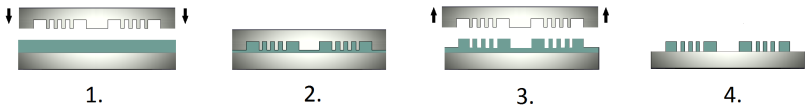

Figure 8: The principle of nanoimprint lithography. A patterned stamp and a resist-coated wafer (1.) are pressed together (2.). While they are in contact the resist is made solid and will retain its shape after separation (3.). The residual layer of resist, in the bottom of imprinted features, is removed (4.)

2.4.2 NIL-stamp

The stamp can either be made of a soft material such as PDMS or in a hard material such as SiO_2. Hard stamps usually have longer life times and better resolution, but fabrication and demolding are often more difficult. The stamp fabrication is the most time consuming part of the fabrication process, since it includes many steps, there among patterning with EBL. However, once a stamp is made, it can be used to imprint many copies of a structure, and the imprinting process itself only takes a few minutes. [19]

An important property of the stamp is the cross section profile of the protrusions, illustrated in Figure 9. An undercut profile will better confine filaments to the channel than a tapered profile, but an undercut will cause problems during separation, since imprinted resist will be trapped in the cavities and will be damaged when pulled off. To facilitate separation, a slightly tapered profile is usually aimed for in NIL [20], but makes it easier for filaments to escape. Therefore a vertical profile should be aimed for in this case. A high aspect-ratio of the channels, prevents filaments from escaping, but cause separation to be more difficult because of the increased contact area between the imprinted material and the stamp. [20]

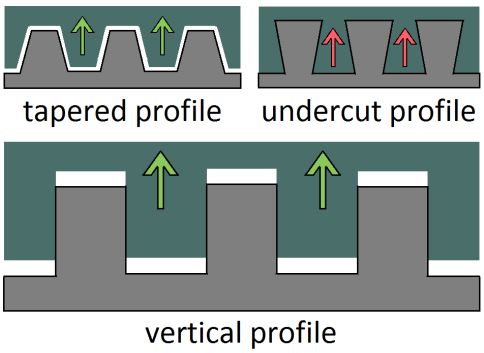

Figure 9: A schematic illustration of three different protrusion profiles in a NIL-stamp. In a NIL process, an undercut profile undesirable, since resist will be trapped in the cavities and the structures will be damaged during separation. A tapered profile is easier to separate, but increase the risk of filaments escaping from the channels. Therefore a vertical profile is aimed for in the fabrication process.

2.4.3 Thermal NIL and UV-NIL

There are two main types of NIL, thermal NIL and UV-NIL. In Figure 10, two graphs are shown, which illustrate the two different processes. In thermal NIL, also called hot embossing, a thermoplastic polymer resist is used as a substrate. The viscosity of a thermoplastic polymer can be altered by changing the temperature and becomes ductile when it is heated. For a thermoplastic polymer, the glass transition temperature T_g is an important feature. T_g is the temperature at which the thermal energy is high enough for polymer chains to be able stretch but too low to allow them to move in relation to one another. Deformation is therefore elastic and reversible.[11] Thus, in thermal NIL, imprinting needs to be conducted above this temperature. [21] At a high temperature and a high pressure, the stamp is pressed into the viscous resist. The temperature is then lowered again, below T_g, so that the resist becomes solid. Thereafter, the stamp can be removed. [11]

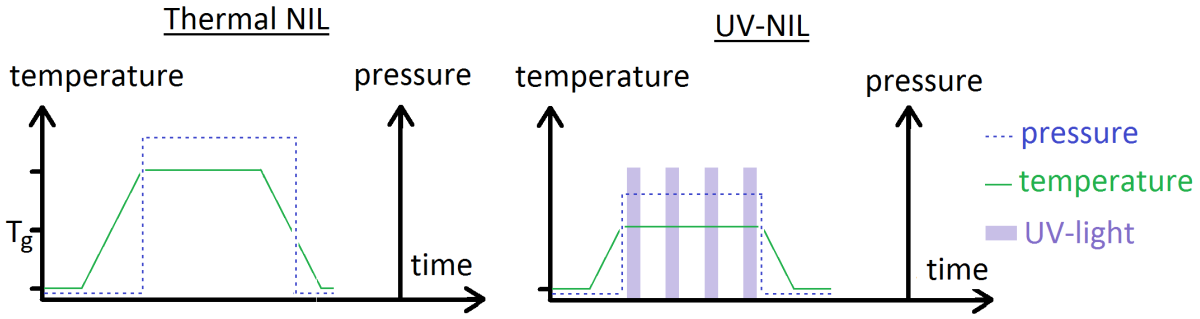

Figure 10: The two graphs show the imprinting process for thermal NIL (left) and UV-NIL (right). In thermal NIL, imprinting is conducted above T_g. In UV-NIL (right), the resist is in a viscous, liquid phase at low temperatures, which is why no/little heating and low pressure is needed. The resist is cured by exposing it to UV-light. To be able to expose the resist, a UV-transparent stamp is needed.

The other main category, called UV-NIL, can be performed in lower temperatures down to room temperature. This is due to that the resist is in a soft viscous state at room temperature. The resist is cured during imprint, by exposing it to UV-light through the stamp and therefore a UV-transparent stamp is needed. The exposure causes crosslinking of polymer chains, making it a solid polymer, which cannot soften again. UV-NIL is often preferred over thermal NIL, since imprinting can be done at lower temperatures, which results in less problems with built-in tensions in the devices and deformation after cooling, due to temperature dependent size changes. [11]

2.4.4 Imprinting process using an intermediate polymer stamp

A variant of a NIL-process separates the imprinting in two steps, by fabricating an intermediate stamp. First, a master stamp is fabricated using EBL. The master stamp is thereafter used to make a soft, transparent, intermediate polymer stamp, an IPS® (Obducat), from a polymer sheet, by a thermal NIL process. In the next step, the IPS is used to imprint devices, with the possibility of using UV-NIL. The imprinting procedure, using an IPS, is illustrated in Figure 11. [22]

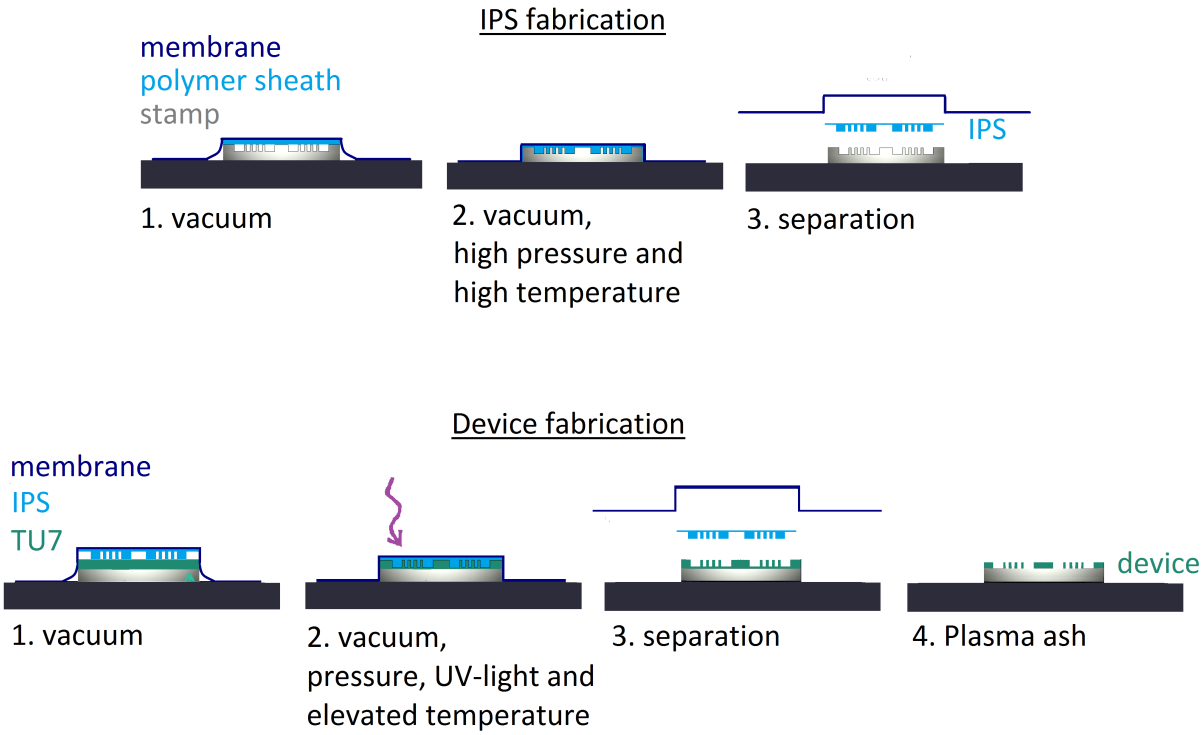

Figure 11: Illustration of a NIL-process using an IPS. The pattern is transferred from the master stamp to the device in two imprinting steps. First an IPS is fabricated with thermal NIL from the master stamp. Then the IPS is used in UV-NIL to imprint the device.

Using an IPS is advantageous for two reasons. First, the process is gentle and reduces the risk of cracking the stamp as it avoids having two hard materials pressed together. Secondly, the IPS can be reused, which reduces the wear of the master stamp, which makes it possible to make more copies from it.[22]

2.4.5 Issues with nanoimprint lithography

A thin residual layer of resist is always left at the bottom of imprinted structures. This layer is in most cases unwanted and has to be removed in an etching process afterwards. Reducing the thickness of the residual layer is therefore important, as a thicker residual layer needs longer etching time, which reduces the resolution of the structures. The thickness of the residual layer depends on the initial thickness of the polymer film and the height of the protrusions in the stamp. It also depends on the fill factor, which is the ratio between areas of intrusions in the stamp and the total stamp area. A higher fill factor will reduce the height of the residual

layer.[11]

The most difficult issue for NIL, is imprinting of both large and small structures and varying distribution of structures in the pattern layout. Significant variations in the pattern lead to a varying height of the residual layer, and/or a varying height of imprinted structures. This is due to the fact that large structures imprinted next to small structures, have to displace more material and displace it longer distances, which leads to an accumulation of resist at the edges of large structures. If the flow away from these areas is insufficient, the accumulated material will hinder the stamp to fully be pressed down, as illustrated in Figure 12. Similarly, large intrusions next to patterned areas, can cause dips in the imprinted resist.[11][21]

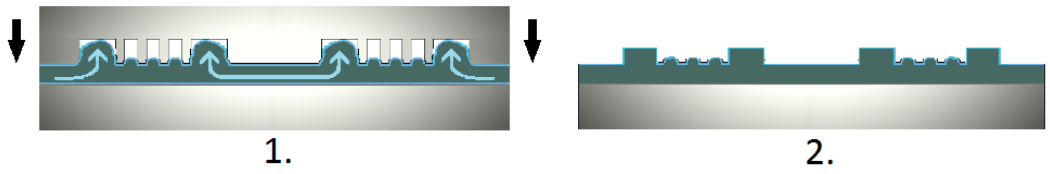

Figure 12: Figure showing a common defect in NIL, caused by having a varying fill factor in the stamp. The smaller, narrower features, is not resolved due the accumulation of material at the edges of larger features.

A lower viscosity of the resist will reduce the defects caused by a varying fill factor by increasing the flow. This can be achieved by imprinting at higher temperature. However, a higher temperature will increase deformations due to thermally dependent size changes. A more dilute resist also result in a lower viscosity, but will increase shrinking of structures when solvent evaporates. A lower viscosity can also be achieved by using a polymer resin with a lower molecular weight. However, this will result in a more brittle material. These factors has to be weighed against each other, when choosing material.[21]

The large contact area between the stamp and the resist can make the separation difficult, since there is a high risk that resist will stick to the stamp instead of the substrate. This leads to structures missing in the device and blocked structures in the stamp. Therefore, the stamp is pre-treated with an anti-adhesive coating which has a low molecular interaction with the imprint resist. A low surface energy-material is therefore desirable, which

also prevents contamination of the stamp. Often a fluorinated trichlorosilane (FTCS) compound is deposited as a thin film on top of the stamp for this purpose. FTCSs have low surface energies and are durable. The anti-adhesive will however eventually be worn down after repeated imprints, and is a limiting factor of the life-time of the stamp.[11]

3 Material testing of TU7

A resist called TU7 (Obducat) was tested as wall material of the structures in the devices. The interaction between TU7 and HMM had to be tested to make sure that TU7 showed no motility of f-actin. Samples with TU7 were prepared and subjected to the same surface treatments as the devices. Motility assays were then performed, which showed that TU7 could be used.

3.1 Sample preparation

70 nm of SiO_2 was deposited with atomic layer deposition (ALD) on a two inch Si(100)-wafer. The wafer was thereafter cleaned by immersing it acetone followed by isopropanol (IPA) for three minutes each. It was then blow dried in N2-gas. Next, TU7 was spin coated ontop of the SiO_2 for 60s at 1500 rpm. The wafer was thereafter baked on a hotplate for one minute at 95 ^{o}C.

The wafer was diced into smaller samples (1x1 cm). Three samples, denoted sample 1 - sample 3, were plasma ashed for 15 seconds. They were subsequently incubated with TMCS vapor in room temperature, for 10, 20 and 30 minutes respectively. One sample, sample 4, was not plasma ashed, but was directly incubated with TMCS for 20 minutes. Table 1 shows a summary of the TU7 samples.

Table 1: Surface treatments on TU7 samples 1-4.

sample	plasma ash, 15 s	TMCS
1	yes	10 min
2	yes	20 min
3	yes	30 min
4	no	20 min

3.2 Motility assays in flow cells

Flow cells were constructed from the four different samples as illustrated in Figure 13. The small void between the glass and the sample was filled with buffer solution, by capillary diffusion. The flow cell liquid was exchanged by depositing solutions with a pipette at one opening and placing an absorbing filter paper at the other, which created a flow through the flow cell. [9][13]

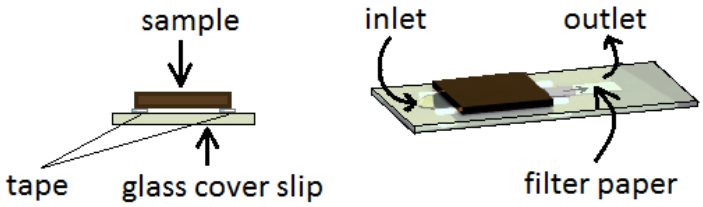

Figure 13: Figures showing the cross section (left) and side view (right) of a flow cell.

The flow cells were incubated for five minutes with a solution containing suspended HMM (120 µg/mL). Thereafter, they were incubated for two minutes with bovine serum albumin (BSA 1 mg/mL) to prevent non-specific binding of f-actin to the surface. Then followed a flow-through of wash solution to remove redundant proteins. Next, the samples were incubated for two minutes with actin filaments (10 nM) labeled with the fluorescent molecule Rhodamine Phalloidin. The samples were protected from light during the incubation, to prevent bleaching of the fluorophores. Subsequently, the samples were washed with buffer solution to remove excess actin filaments, and finally the samples were incubated for two minutes with an ATP-containing solution. The flow cells were thereafter studied with fluorescence interference contrast microscopy, FLIC-microscopy, to study the motility of f-actin on the samples.

3.3 Results from motility assays

No motility was observed for the plasma ashed samples 1-3. On sample 4 motility was seen. Thus, plasma ashing is necessary both for removing the residual layer of TU7 after imprinting, and to suppress motility by making the surface hydrophilic. 15 s plasma ashing and 20 minutes TMCS-exposure (same as sample 2) have previously been used for devices. As no motility was observed for sample 2, these surface treatments were decided to be kept for NIL-fabrication of new devices.

4 Loading zone design and wafer layout

The aspect ratio between height and width of the open loading zones is very small and the size difference between the loading zones and the nanochannels is very large. These properties made NIL difficult. Therefore it was necessary to change the design of the loading zones to be able to imprint the structures.

The loading zones have two purposes that needed to be considered when redesigning them. First, they are needed as a capture area when filaments are added to the buffer. The filaments need to reach the HMM-coated floor by diffusion to bind in. It is improbable that several μm long filaments, which are constantly moving and bending, enter the 200 nm wide nanochannels uncompelled. Thus, a large area is needed to capture them. Secondly, after the filaments have bound to the HMM-surface, the loading zones should guide the filaments into the exit nanochannel.

4.1 Pattern design

The drop shape of the loading zones was kept in the new designs. However, structures were added to the open space in different patterns. The patterns had to leave enough space between the structures so that filaments still could diffuse easily to the floor.

Patterns were designed in Raith150 EBL software combined with the design software L-Edit. 55 different loading zones were drawn. The pattern structures had diameters of 2-9 μm, to be in same order of size as the length of the filaments (a few μm). Different shapes of features, such as triangles and circles were designed, as well as different layouts and different fill factors. Three main types of loading zones were used, which can be compared in Figure 14. The zone1-type had a smooth outline as previous loading zones. The zone2-type had a spiky outline, to direct filaments away from the edge and into the pattern. Finally, the zone3-type had an open, non-patterned area at the top. The small non-patterned area was kept to facilitate for filaments diffuse down to the HMM coated floor. All loading zone designs can be seen in Appendix A.

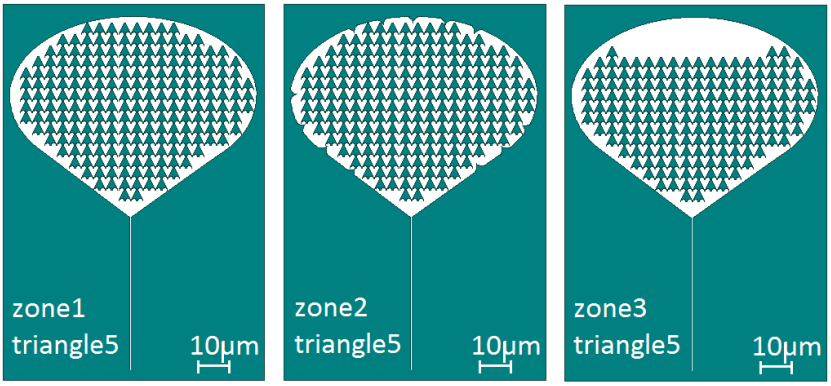

Figure 14: Comparison of the three main types of loading zones for the pattern triangle5.

4.1.1 Simulations

Filament motility was simulated in Matlab (by Till Korten, TU Dresden). 500 filaments were randomly distributed in the 2D loading zone patterns and simulated to move randomly. In the simulations it was presupposed that filaments had been able to bind in to the HMM-surface. Their motions were restricted by their persistence length (10 μm), the pattern and the outline of the loading zone. The simulation did not take into account the length of the filaments or that an area might already be crowded by other filaments. After they entered the exit nanochannel, they were removed from the simulation.

4.1.2 Results and discussion of simulations

The simulations indicated that f-actin could be guided towards the exit nanochannel by the patterns. Naturally, they could also be steered in any other preferable direction. Different loading rates could be achieved by varying the pattern. Activity maps and plots of the loading rate were obtained from the simulations. An activity map is an summation image of the whole simulation time span. It shows how frequent a point in the loading zone has been visited by filaments with the use of a color scheme. The more occasions, the brighter color is assigned to it. An example of an activity map for loading zone z2_drop1_1 is shown in Figure 15. As can be seen in the figure, the area towards the exit nanochannel has been visited by filaments more often than the top of it. Thereby the loading rate were increased compared to a non-patterned loading zone. All activity maps can be seen in Appendix A.

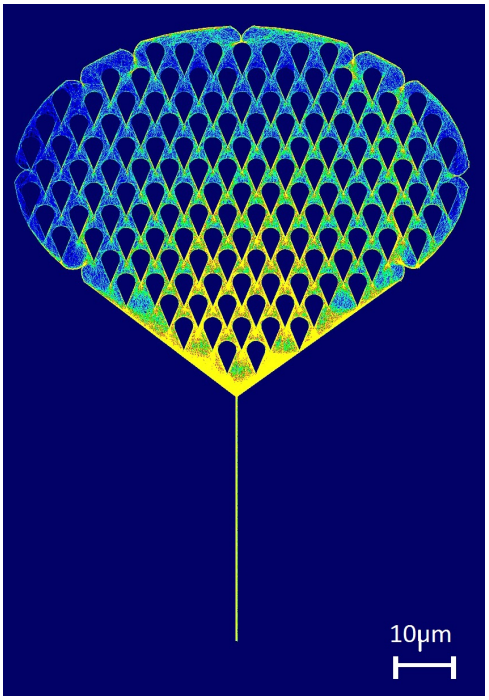

Figure 15: Activity map of loading zone z2_drop1_1. The activity map was obtained from motility simulations of f-actin (by Till Korten, TU Dresden). Brighter areas have been visited more often.

The plots of the loading rates can be studied to compare different patterns. The shape as well as the placement of structures affected the rate. As an example, z1_drop1_1 and z1_drop1_2 have the same shape of structures, but have a different layout. The difference in layout resulted in filaments moving in opposite directions. This had a clear effect on the loading rate, as can be seen in the plot in Figure 16 a) where the two loading zones are compared. An other example can be seen in Figure 16 b), where z1_triangle2_1 and z1_triangle2_2 are compared. They also have the same shape of structures, with the difference that the structures in z1_triangle2_2 are placed closer together. This did not seem to affect the loading rate markedly as can be seen in the plot. In Figure 16 c), the loading rates of zone 1, zone 2 and zone 3 are compared for the pattern figure2. No significant difference in loading rate could be seen between the three. The most time efficient pattern was triangle5 (see Figure 16 d)), which is composed of heart shaped structures, each acting as a rectifier of filaments towards the opening of the exit nanochannel. The loading rates for the plotted patterns are summarized in Table 2

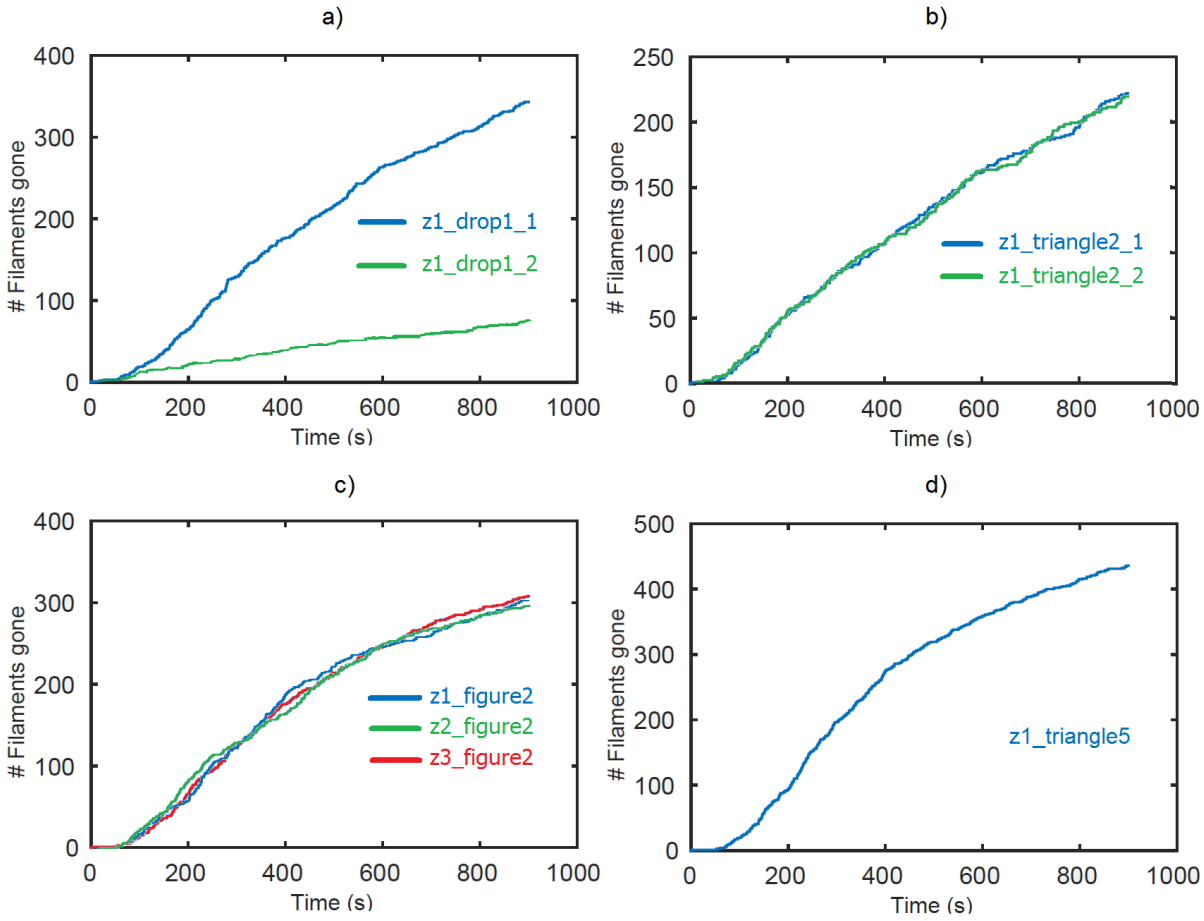

Figure 16: Graphs showing loading rates of different loading zones, with number of filaments that have entered the nanochannel on the y-axis, versus time in seconds on the x-axis. Note that the scale on the y-axis is different in a)- d).

Table 2: The pattern designs and their corresponding loading rates of the plotted patterns in Figure 16.

Name:	Figure 16 a) z1_drop1_1	z1_drop1_2	Figure 16 b) z1_triangle2_1	z1_triangle2_2
	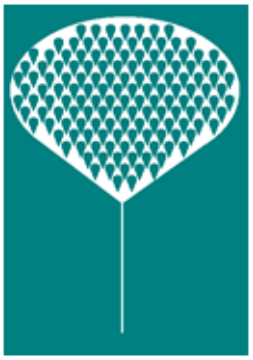		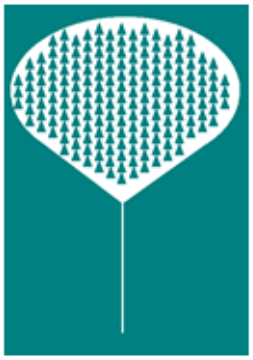	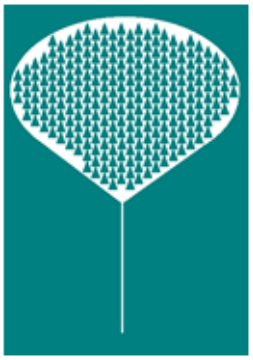
Rate:	0.39 filaments/s	0.08 filaments/s	0.25 filaments/s	0.25 filaments/s
Name:	Figure 16 c) z1_figure2	z2_figure2	z3_figure2	Figure 16 d) z1_triangle5
				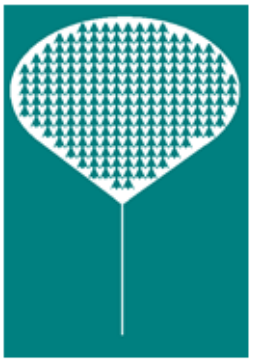
Rate:	0.34 filaments/s	0.33 filaments/s	0.34 filaments/s	0.48 filaments/s

The simulated velocity of filaments was slower than their velocity in vitro (up to 10μm/s) [9]. However, the time scale do not affect the path of the filaments in the simulations, and does therefore not affect the appearance of the activity maps. The x-axis time scale in the plots should be divided by a factor of 5-10 to better represent an experiment in vitro. In a device, the filaments should be fed into the exit nanochannel at an even, but fast pace, and optimally one by one. If assuming a filament length of 5 μm and a filament speed of 10μm/s, a good rate would be two filaments entering the exit nanochannel per second. By doing a rough estimation, this speed could for example be achieved with z1_triangle2_1 and z1_triangle2_2 in Figure 16 b), which have a loading rate of approximately 200 filaments per 100 seconds (dividing the time axis with a factor of 8). Of course there are many factors that can affect the rate and perhaps a faster or slower

pattern turns out to be better suited. A pattern with very slow rate, such as z1_drop1_2 in Figure 16 a), could instead be used if one would like to follow the track of a single filament.

All aspects of the movements of filaments were not taken into account in the simulations. The movements of filaments are a result of a combination of random motion due to thermal fluctuations, and the work by and distribution of HMM. There might be molecular interactions between walls and filaments or between walls and HMM, which could affect their distribution and there could be a buildup of filaments in crowded areas, hindering them to move forward and clogging the device.

Some artifacts in the activity maps are present, which occur because filaments occasionally move across solid features. This is due to that the simulation step size exceeds the thickness of the narrowest features.

The ability of capturing filaments to the HMM-coated loading zone floor is an important property, but is not tested in the simulations. Therefore, the possible advantage of having a zone3 could not be seen. Similarly could the capturing capabilities of more open versus more dense patterns not be compared. Instead this needs to be investigated in motility assays. If the patterned loading zones turn out to slow down the capturing of filaments due to the decreased space, the overall loading zone area could be increased to compensate for this.

4.2 Wafer lay-out

Loading zone patterns were selected from the result of the simulations. Patterns with different loading rates were chosen. A comparison between the ratios of fast versus slow loading zones in vitro, with the same ratio in the simulations, could be used as an indication of how well the simulations represent the reality. Patterns with identical structures but with different fill factors, such as triangle2_1 and triangle2_2, were selected. They could be studied to compare how the difference in fill factor affects the quality of the imprint, the capturing capabilities and the loading rate. Patterns with the three different variants of zones (zone1, zone2 and zone3) were selected to compare their loading rates and capturing capabilities.

Feedback loops, illustrated in Figure 17, were added to those loading zones

that were chosen to be imprinted. The feedback loops guide f-actin from the exit nanochannel, back to the loading zone, to not block the structures during motility assays. The statistical data of the loading rate is also improved by recycling the filaments.

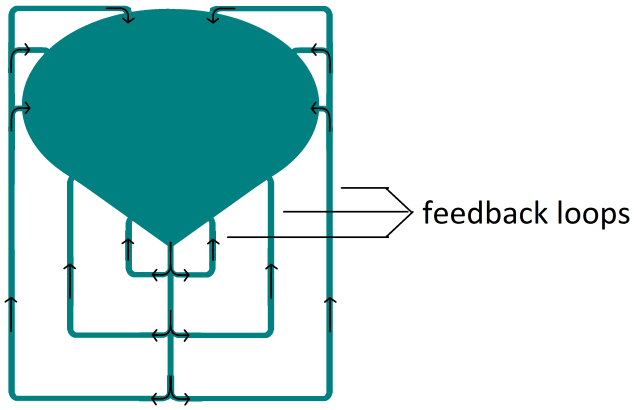

Figure 17: Filaments that have entered the exit nanochannel are guided back into the loading zone by feedback loops.

A two inch lay-out was made for on a four inch wafer with EBL. The reason for using a four inch wafer was to avoid edge defects during the deposition- and etch-steps. Normally the center of the wafer is more evenly processed.[23][24] The wafer layout was divided into 16 sub-samples of 1x1 cm^2, as can be seen in Figure 18 (left).

Table 3: Pattern layout in samples

sample		pattern row1	pattern row2
1:1,	2:1	z1_triangle5	z1_triangle6_1
1:2,	2:2	z2_circle2	z2_drop1_1
1:3,	2:3	z2_figure2	z2_triangle5
1:4,	2:4	z3_figure2	z3_triangle2_1
1:5,	2:5	z3_triangle5	LZ1/LZ2
1:6,	2:6	z1_circle2	z1_drop1_1
1:7,	2:7	z1_figure1	z1_figure2
1:8,	2:8	z1_triangle2_1	z1_triangle2_2

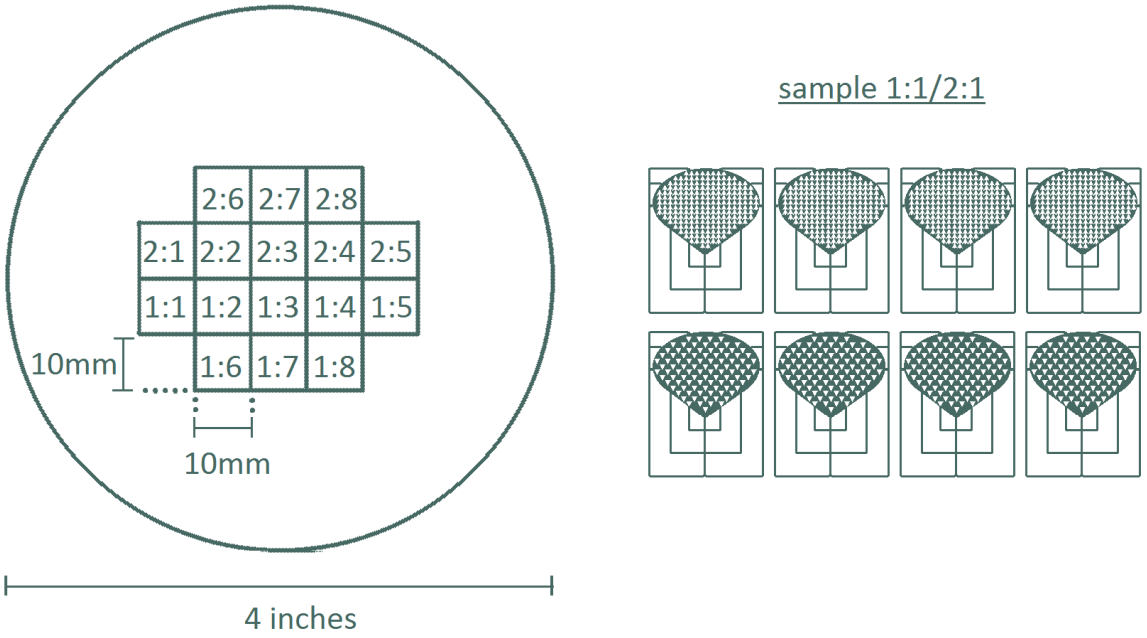

Figure 18: To the left is an illustration of the wafer layout on a 4 inch wafer. The center of the wafer was divided into 16 sub-samples. Each sub-sample contained two rows of four loading zones, as shown in the illustration to the right.

The 16 samples each contained two rows of 4 loading zones, as illustrated in Figure 18 (right). Two copies of each sample was made. Sample 1:1 was identical to sample 2:1, sample 1:2 was identical to 2:2 etc. The layout of each sample is presented in Table 3.

5 Master stamp fabrication

A Si(100) four inch wafer was used as a substrate for the master stamp. The structure pattern was defined in a layer of SiO_2 on top of the Si substrate. Several steps of thin film deposition, EBL patterning and etching, were needed to pattern the SiO_2. Thereafter, the master stamp was anti-sticking treated.

5.1 Deposition of SiO_2 and etch mask

Plasma enhanced chemical vapor deposition (PECVD) was used to deposit a layer of approximately 300 nm of SiO_2 (with SiH_4 and N_2H used as precursors). This layer would later be the patterned surface of the stamp. On top, thin films of other materials were deposited to fabricate an etch mask. First, 60 nm Cr was deposited using thermal physical vapor deposition (PVD). Next, 30 nm of SiO_2 were deposited with ALD. The wafer was thereafter cleaned by immersing it acetone followed by isopropanol (IPA) for three minutes each. It was then blow dried with N2-gas. Last, approximately 250 nm [25] of ARP6200.09 (positive e-beam resist, Allresist GmbH) was spin coated on top for 30 s at 3000 rpm. The wafer was thereafter baked on a hotplate for two minutes at 160 ^oC. The layered structure of the master stamp during fabrication, is illustrated in Figure 19.

Figure 19: Illustration of the master stamp during fabrication. A 300 nm SiO_2 layer was deposited on a Si wafer. This layer would later serve as the patterned surface of the master stamp. An etch mask consisting of three layers, was thereafter deposited, which included 60 nm Cr, 30 nm SiO_2 and 250 nm AR-P6200-09 resist.

5.2 EBL exposure of master stamp

The wafer was exposed with EBL to define the pattern in the top resist layer. The following exposure parameters were used: Dose = 60 uC/cm2,

step size 20x20 nm

Acceleration voltage: 20 kV

Aperture: 20 μm

Dose: 60 μC/cm^2

Step size: 20x20 nm^2

The wafer was developed in ortho-xylene for five minutes during which exposed resist was dissolved, uncovering the SiO_2-layer underneath. Excess developer was rinsed off by immersing the wafer in IPA and subsequently blow drying it with N_2.

5.3 Master stamp etching

Next step was to transfer the pattern into the thick SiO_2. This was done in a series of etching steps, as illustrated in Figure 20. Inductively coupled plasma reactive-ion etching (ICP-RIE) was used to etch the master stamp. A combination of O_2- and C_4F_8-plasma were used to etch SiO_2, and O_2- and Cl_2-plasma were used to etch Cr and resist. After ICP-RIE, the remaining Cr was removed by immersing the wafer in the inorganic solvent Chrome Etch 18 for five minutes. The wafer was subsequently immersed in water for five minutes, thereafter rinsed in running water for approximately one minute, followed by N_2-blow drying. The EBL and etching steps are illustrated in Figure 20

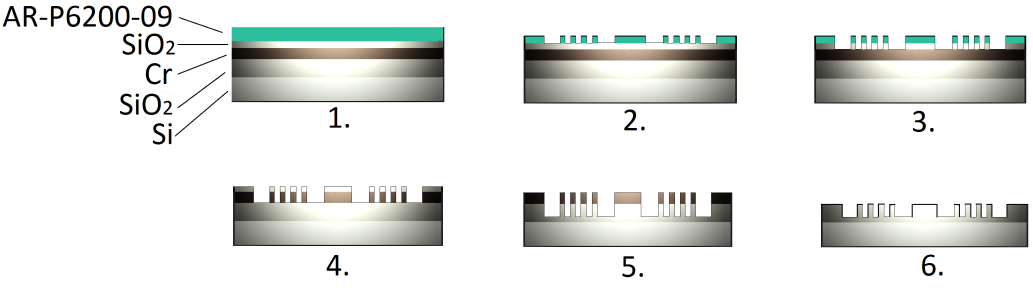

Figure 20: The EBL and etch steps of the master stamp fabrication. 1. The wafer is exposed with EBL. 2. The pattern is developed. 3. The pattern is etched down in the top SiO_2 with ICP-RIE by O_2- and C_4F_8-plasma. 4. The pattern is etched down in the Cr with ICP-RIE by O_2- and Cl_2-plasma. 5. The pattern is etched down in the bottom SiO_2 with ICP-RIE by O_2- and C_4F_8-plasma. 6. The Cr is removed by wet etching in Chrome Etch 18.

5.4 Anti-sticking treatment of master stamp

The master stamp was surface treated with an anti-adhesive coating to lower the surface free energy. A lower surface free energy is desired, since it reduces the adhesion to an imprinted polymer. [26] The master stamp was exposed to FDTS-vapor (Fluorodecyltrichlorosilane-vapor) in an ALD-chamber for 47 minutes, followed by an additional 22 minutes. FDTS forms a monolayer with covalent [Si-O-Si]-bonds to an SiO_2-surface. FDTS has a low surface free energy due to its fluorinated tail groups.[27]

A lower surface free energy increases the contact angel to a drop of water. [28] Contact angle measurements to water on the surface treated master stamp was therefore used to determine if the coating had been successful. This was done by comparing measured contact angles with contact angles for FDTS found in literature, which is on average 100° [27]. After the second run, the contact angle was measured to be 107°-109° (thus indicating an even lower surface free energy than the average value). This meant that the coating was successful.

5.5 Results and discussion of master stamp fabrication

The thickness of the bottom layer of SiO_2 was measured with ellipsometry to be 373 nm, thus thicker than the expected 300 nm. However, a thicker SiO_2 bottom layer do not affect the quality of the imprint, since the etching of this layer is stopped at the desired depth anyway.

The EBL exposure was problematic due to the complexity of the patterns. The software could not read the all files correctly even though the structures appeared fine in the preview in the program. This resulted in samples being only partly exposed and samples containing systematic defects. This problem could possibly have arose due to that the files were converted between different file formats. The conversion was needed as Raith150 missed necessary functions. Designing the patterns thus required working in two different software. This problem will remain if continuing to use the Raith150 software in future fabrication.

The stamp was studied in an optical microscope after the FDTS-treatment. In Figure 21, sample 2:6 is shown. The horizontal lines across the two

bottom pictures arose from merging two images.

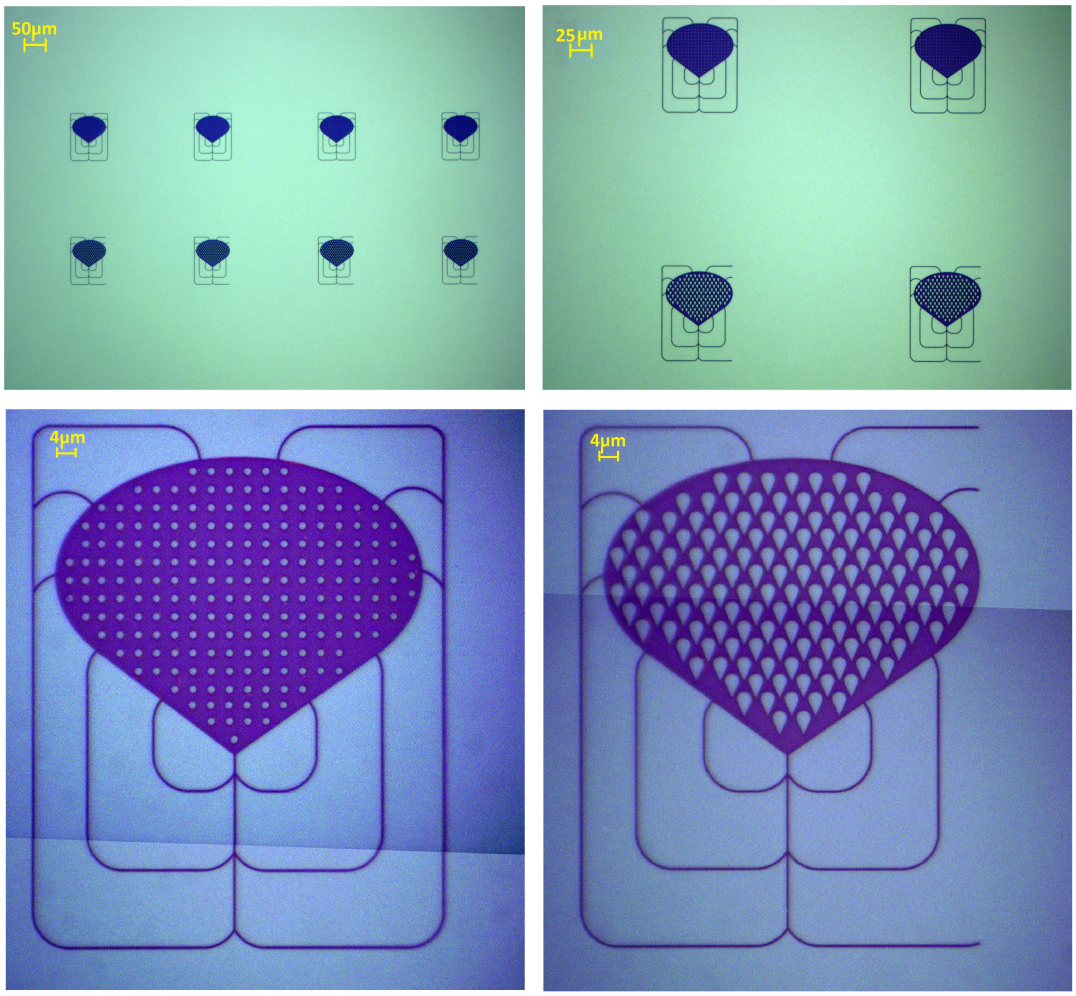

Figure 21: Figure showing sample 2:6 in the master stamp. Top images: Overviews of the sample. Bottom left image: row1, z1_circle2. Bottom right image: row2, z1_drop1_1.

Too small distances between features can cause them to merge. This can be seen in the encircled area of Figure 22, between the spiky edge and the drop pattern. To avoid this, the distance between features should be set to at least 200 nm.

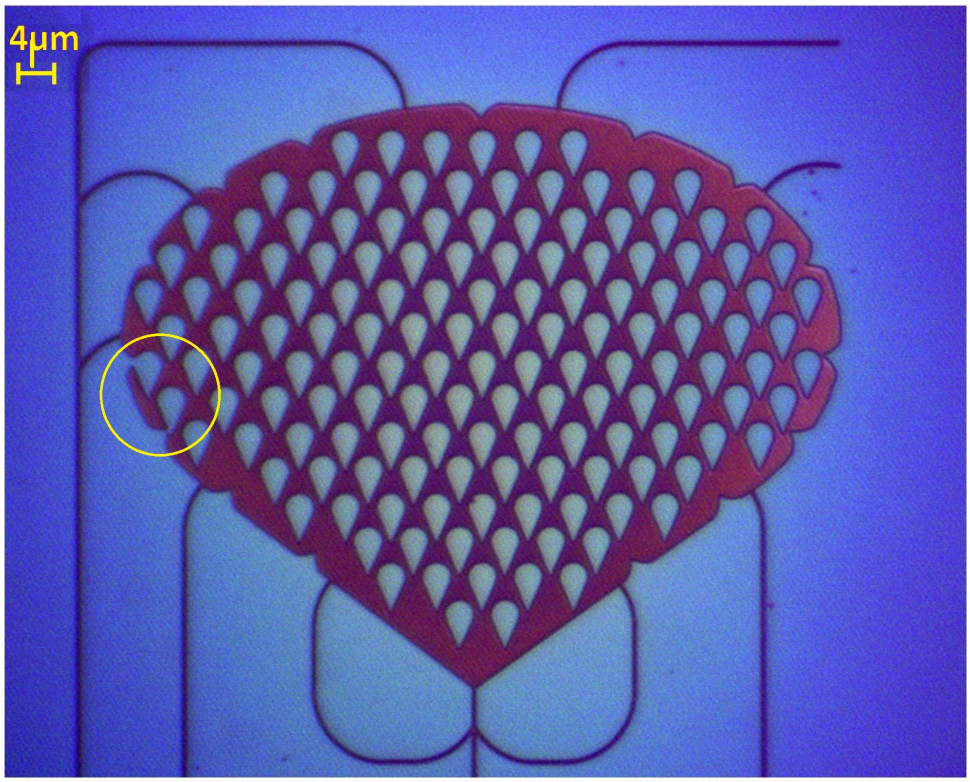

Figure 22: z2_drop1_1 in the master stamp. Features close to each other have merged, as can be seen in the marked area.

6 Nanoimprint lithography

6.1 IPS fabrication

The master stamp was placed on a perforated carrier plate with the pattern facing up. It was held in place by pumping vacuum through the carrier plate. An IPS polymer sheet was placed on top of the master stamp, a transparent membrane covered them both and an O-ring fixated the whole arrangement. Outer holes in the carrier plate were used to evacuate the air from the enclosed package. The use of a membrane and an O-ring reduces the volume that needed to be evacuated from air and also keeps the environment of the stamp clean.

The temperature was increased to 160 ^{o}C, after which compressed air was used to create an even pressure of 50 bar across the membrane, which pressed down on the IPS and master stamp. After 2 minutes, the temperature was lowered to 115 ^{o}C. Subsequently, the pressure was lowered to ambient pressure and the vacuum pump was turned off. The IPS could thereafter be removed from the master stamp by carefully pulling it off.

6.2 Imprinting devices by UV-NIL

A two inch Si wafer was plasma ashed for 3x1 minutes to activate the surface for better adhesion of TU7. It was thereafter directly spin coated with TU7 for 60 s at 1500 rpm. Subsequently, the wafer was baked on a hotplate for one minute at 95 ^{o}C.
The TU7-coated wafer was imprinted using the IPS. The wafer was placed on the carrier plate with the IPS on top. A membrane and an O-ring were used to encapsulate them, and the package were evacuated from air. The temperature was increased to 75^{o}C. A pressure of 20 bar was thereafter applied, during which the wafer was exposed to UV-light in 4x5 s pulses (10 s in between). Pressure and temperature were held for two minutes after which they were lowered to ambient conditions. The IPS could then be removed by carefully pulling it off.

6.3 Results and discussion of IPS fabrication and device imprinting

The pattern transfer to the IPS appeared to be successful from what could be seen in an optical microscope. However, topographic information from the IPS could not be acquired from these images. Therefore it should be studied in a scanning electron microscope (SEM) by using a low acceleration voltage or by first sputtering it with a metal coating. Alternatively, it can be studied in an atomic force microscope (AFM).

Si wafer should have been coated with 70 nm of SiO_2 before spin coating it with TU7. However, this was accidentally forgotten in the process. This probably did not affected the imprinting, but excluded the possibility of using FLIC-microscopy in motility tests later on. Therefore new imprints should be done before motility assays can be performed.

In Table 4, optical microscope images of the imprinted devices are shown. Some samples are completely unexposed (1:1, 1:2, 1:8) and are therefore missing in the table. Some samples only contain one row (1/2:3, 1/2:4 and 1/2:7) and some samples are missing parts of their patterns (see for example 2:1 row2 and 1:4 row1). These defects were caused by the software issues. Other type of defects are also present. In 2:4: row1, traces of large impurities can be seen, which was there already in the master stamp. However, smaller particle impurities are more abundant. For the large

open areas such as in Figure 23 a), the color shifting indicates that the imprint is uneven with a varying thickness of the residual layer. The patterned loading zones and their nanochannels are generally well resolved (see Figure 23 b) and c)). Even the smaller open areas of zone 3 type of patterns (see Figure 23 d)), seem to be possible to imprint with a good result.

Table 4: The result of each sample after UV-NIL of TU7 is shown below. Many samples are missing structures due to software issues with the EBL system.

Sample	Row1	Row2	Sample	Row1	Row2
1:1			2:1	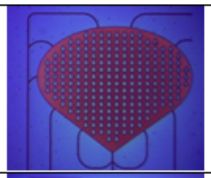	
1:2			2:2	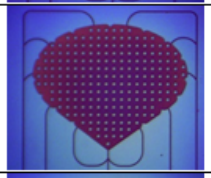	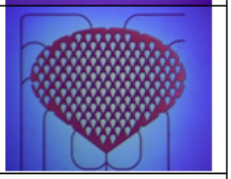
1:3	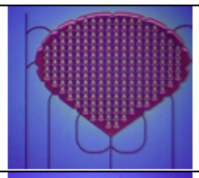		2:3	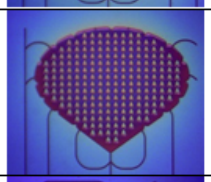	
1:4	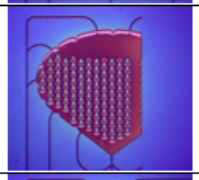		2:4	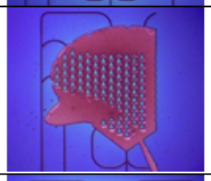	
1:5	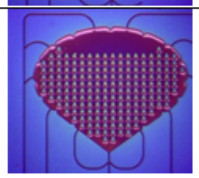	 	2:5	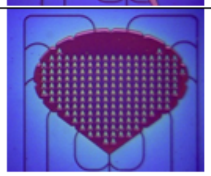	 
1:6	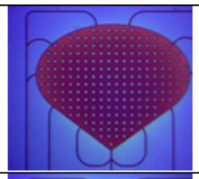	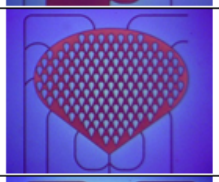	2:6	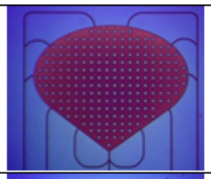	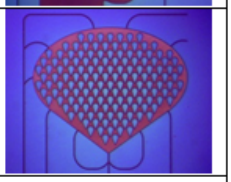
1:7	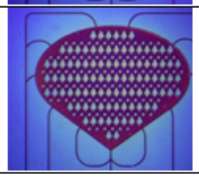	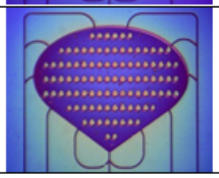	2:7		
1:8			2:8	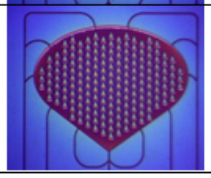	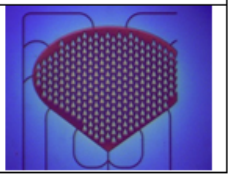

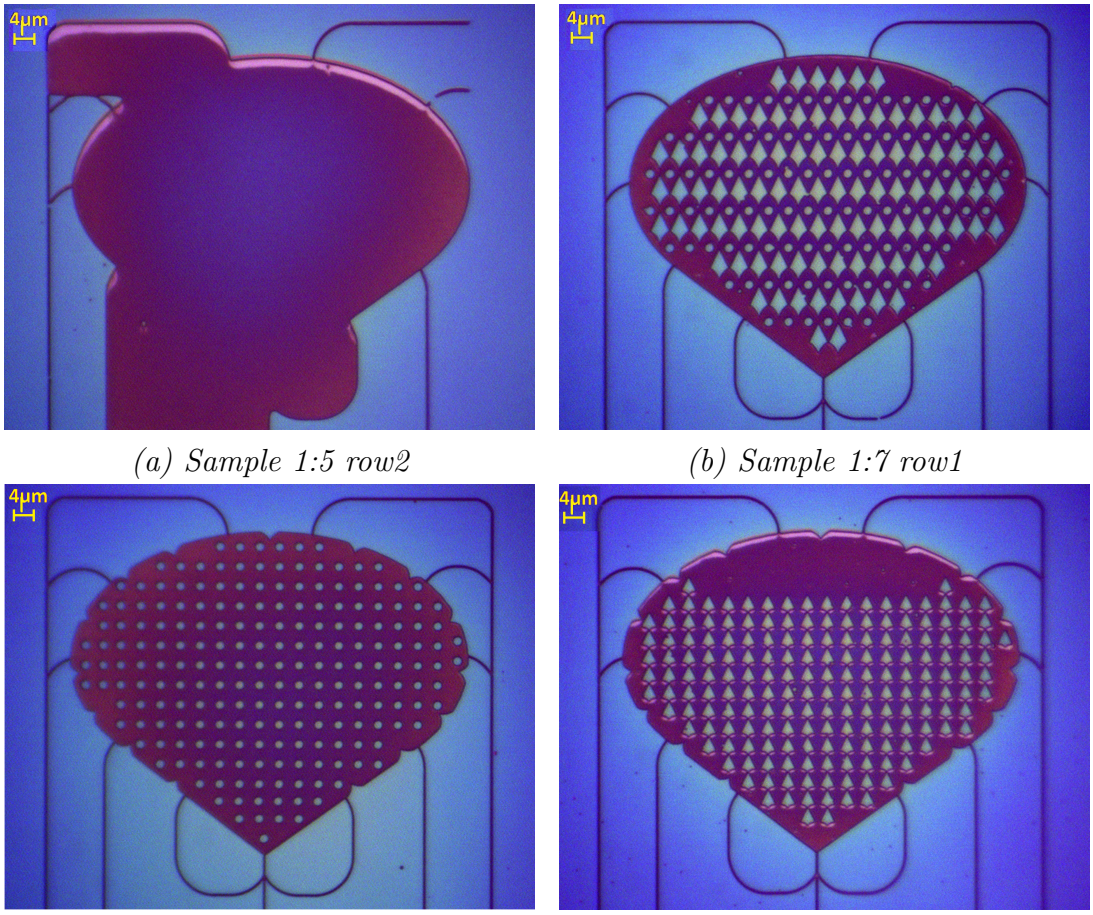

(a) Sample 1:5 row2

(b) Sample 1:7 row1

(c) Sample 2:2 row1

(d) Sample 1:5 row1

Figure 23: Imprinted devices with different patterns are shown above. As can be seen an example of in a), some of the samples are missing parts of the patterns. Apart from this, the patterned loading zones in b), c) and d) show an even result with well resolved pattern structures and nanochannels. The completely open loading zone in a) appears on the contrary to be uneven.

To be able to analyze the result in more detail, the devices should be studied in a SEM or AFM to acquire topological information. By doing so, variations in structure heights and residual layer thickness can be measured.

7 Conclusions

In this project, nanochannels and loading zones, which are two important components of molecular-motor-based devices, have been fabricated with NIL. The aim of this approach is to open up for future mass production of these devices.

It was determined that TU7, exposed to 15 s plasma ash and 20 min TMCS, could be used as structure wall material in the devices. This was concluded from the results of motility assays, which showed that no motility of f-actin could be observed on TU7.

The open space of the loading zones had to be patterned to reduce the difference size compared to the nanochannels. This was required to make NIL fabrication possible. The patterns could add functionality to the loading zones by varying the loading speed of filaments into the exit nanochannel. This was tested in simulations in Matlab.

Imprinting of devices showed that NIL can be used to fabricate molecular-motor-based devices. The topography of the imprinted devices needs to be further investigated so that the thickness of the residual layer and height of imprinted structures can be measured. This will give more information on the quality if the imprints.

8 Outlook

The next step in this project is to study the imprinted structures in more detail in SEM or AFM. This will give information about the topography. It is then possible to study how different fill factors affect the quality of the imprints. New imprints on Si/SiO_2-wafers coated with TU7 should be made, to be able to perform motility assays on the new structures. Motility assays are important to be able to determine if the patterns perform as in the simulations. They are also important to acquire information about how well filaments are able to bind in to the HMM-coated surfaces, since this is not tested in the simulations. The motility assays will show if the patterning cause any troubles, such as letting filaments escape the HMM-surface, or if it causes filaments to clog up the loadingzone. These results will give an idea of which patterns work the best and how they can be modified to function better. Modifications could include positioning the edge spikes to steer the filaments in to different parts of the patterns, or changing the layout of structures so that filaments are kept in the loading zone for longer/shorter times.

Further into the future, whole devices, with the nanochannel network included, should be imprinted. Thereafter, patterns that cover whole wafer areas should be tested, to see if it is possible to achieve an even result over

larger areas with NIL.

References

[1] Cooper, G. M. (2007) *The cell: a molecular approach*, 4th ed., Washington, D.C.: ASM Press.

[2] Hess, H. (2011) *Engineering applications of biomolecular motors*, Annual Review of Biomedical Engineering, 13, pp. 429–450.

[3] Lin, C.T., Kao, M.T., Kurabayashi, K., Meyhofer, E. (2008) *Self-contained biomolecular motor-driven protein sorting and concentrating in an ultrasensitive microfluidic chip.*, Nano Letters, 8, pp. 1041–1046

[4] Bull, J.L., Hunt, A.J., Meyhofer E. (2005) *A theoretical model of a molecular-motor-powered pump*, Biomedical Microdevices, 7, pp. 21–33.

[5] Song, W., He, Q., Cui, Y., Möhwald, H., Diez, S., Li, J. (2009) *Assembled capsules transportation driven by motor proteins*, Biochemical and Biophysical Research Communications, 379(2), pp. 175-178

[6] Nicolau, D.V. Jr., Lard, M., Korten, T., van Delft, F.C., Persson, M., Bengtsson, E., Månsson, A., Diez, S., Linke, H., Nicolau, D.V. (2013) *Parallel computation with molecular-motor-propelled agents in nanofabricated networks*, Proceedings of the National Academy of Sciences, 113(10), pp. 2591-2596.

[7] Bunk, R., Klinth, J., Rosengren, J., Nicholls, I. ,Tågerud, S., Omling, P., Månsson, A., Montelius, L. (2003) *Towards a "nano-traffic" system powered by molecular motors*, Microelectronic Engineering, 67-68 pp. 899–904

[8] Bunk, R., Sundberg, M., Månsson, A., Nicholls, I.A., Omling, P. Tågerud, S., Montelius, L. (2005) *From milliLiters to nanometers- A nanoscale toolbox for molecular-based transportation.*

[9] Lard, M. (2014) *Nanofabricated devices based on molecular motors biosensing, computation and detection*, Lund: Media-Tryck, Lund University

[10] Mohammad, M. A., Muhammad, M., Dew, S. K., Stepanova, M. (2011) *Fundamentals of Electron Beam Exposure and Development*, in Dew, S. K., Stepanova, M. (ed.) Nanofabrication, techniques and principles. New York: Springer, pp. 11–41

[11] Schift, H., Kristensen, A. (2010) *Nanoimprint Lithography – Patterning of Resists Using Molding*, in Springer Handbook of Nanotechnology. Berlin Heidelberg: Springer, pp. 271-312.

[12] Bunk, R., Månsson, A., Nicholls I. A., Omling, P., Sundberg, M., Tågerud, S., Carlberg, P., Montelius, L. (2005) *Guiding molecular motors with nano-Imprinted structures*, Japanese Journal of Applied Physics, 44(1, 5A)

[13] Kron, S. J., Toyoshima, Y.Y., Uyeda, T.Q., Spudich, J.A. (1991) *Assays for actin sliding movement over myosin-coated surfaces.*, Methods in Enzymology, 196, pp. 399-416.

[14] Bengtsson, E., Persson, M., Månsson, A. (2013). *Analysis of flexural rigidity of actin filaments propelled by surface adsorbed myosin motors.* Cytoskeleton, 70(11), pp.718–728.

[15] Bunk, R., Sundberg, M., Månsson, A., Nicholls, I.A., Omling, P., Tågerud, S., Montelius, L. (2005) *Guiding motor-propelled molecules with nanoscale precision through silanized bi-channel structures*, Nanotechnology, 16(6).

[16] Kron, S. J., Spudich, J. A. (1986) *Fluorescent actin filaments move on myosin fixed to a glass surface*, Proceedings of the National Academy of Sciences, 83, pp. 6272-6276.

[17] Sugimura, H., Nakagiri, N. (1995). *Area-selective formation of an organosilane monolayer on silicon oxide nanopatterns fabricated by scanning probe anodization* Applied Physics Letters, 66(26), pp. 3686.

[18] Nicolau, D. V., Solana, G., Kekic, m., Fulga, F., Mahanivong, C., Wright, J., dos Remedios, C. G. (2007) *Surface hydrophobicity modulates the operation of actomyosin-based dynamic nanodevices*, Langmuir, 23, pp. 10846-10854.

[19] Lan, H., Ding, Y. (2010). *Nanoimprint Lithography*, in Lithography, Michael Wang (ed.), InTech, pp. 457-489, Available at: *http://www.intechopen.com/books/lithography/nanoimprint-lithography* (Accessed: 2016-08-01).

[20] Cui, Z. (2008) *Nanofabrication: Principles, Capabilities and Limits*, Berlin: Springer, cop.

[21] Guo, L. J. (2004) *Recent progress in nanoimprint technology and its applications*, Journal of Physics: Division of Applied Physics, 37(), pp. R123–R141.

[22] OBDUCAT AB, *Technology*, Available at: http://www.obducat.com/Technology-81.aspx (Accessed: 20th of June 2016).

[23] Engelhardt, M. (1994) *Optimized high rate deep silicon trench etching for dielectric isolation in smart power devices*, in Mathad, G. S., Hess, D. W. (ed.) Proceedings of the Tenth Symposium on Plasma Processing. USA: The Electrochemical Society, Incorporated, pp. 224-235

[24] Xiuhua, F., Lin, L., Gibson, D., Waddell, E., Wingo, L. (2013) *Modelling and optimization of film thickness variation for plasma enhanced chemical vapour deposition processes*, Chinese Optics Letters, 11, pp. S10209-1 - S10209-5.

[25] Allresist (2014) Positive E-Beam Resists AR-P 6200 (CSAR 62), Available at: http://www.allresist.com/wp-content/uploads/sites/2/2014/03/allresist_produktinfos_ar-p6200_englisch.pdf (Accessed: 21st of June 2016).

[26] Fillman, R.W., Carroll, J., Krchnavek, R.R. (2009). *Toward a universal anti-stick layer for nanoimprint lithography imprinters: ultra-thin F-DLC*, IEEE Nanotechnology Materials and Devices Conference, Traverse City, Michigan, USA, June 2-5, 2009, pp.186-189.

[27] Pellerite, M.J., Wood, E.J., Jones, V.W. (2002) *Dynamic contact angle studies of self-assembled thin films from fluorinated alkyltrichlorosilanes*, The Journal of Physical Chemistry B, 106, pp. 4746-4754.

[28] Żenkiewicz, M. (2007) *Methods for the calculation of surface free energy of solids*, Journal of Achievements in Materials and Manufacturing Engineering, 24(1), pp. 137-145.

Appendix A

The appendix shows a table of the different pattern designs of loading zones. The purple images show the designed patterns and in the next column, the corresponding activity maps are shown (for those, which were simulated). The left most column shows which pattern is shown, and the top row, shows which type of zone is used:

	ZONE 1	ZONE 1	ZONE 2	ZONE 2	ZONE 3	ZONE 3
Zone 1/2	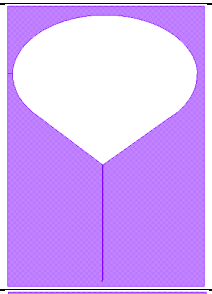	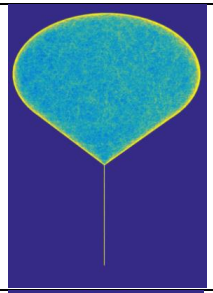	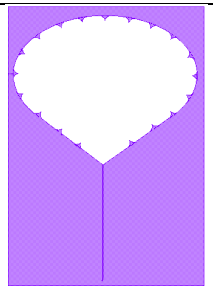	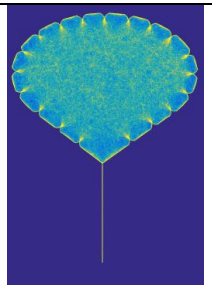		
Circle 1	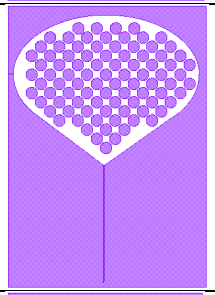	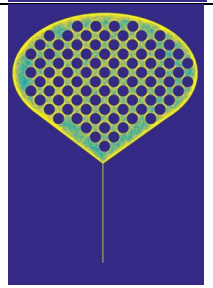	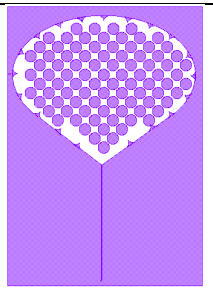	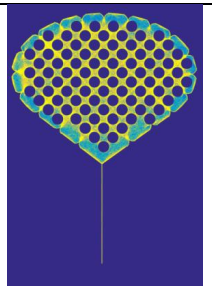		
Circle 2	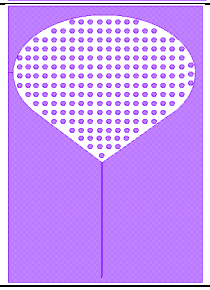	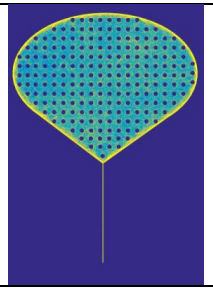	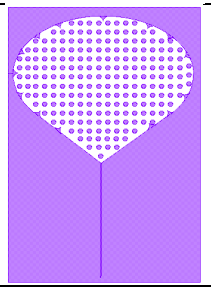	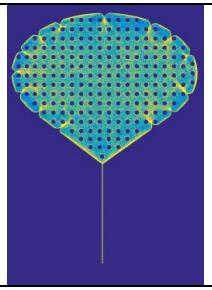		

	ZONE 1	ZONE 1	ZONE 2	ZONE 2	ZONE 3	ZONE 3
Circle 3	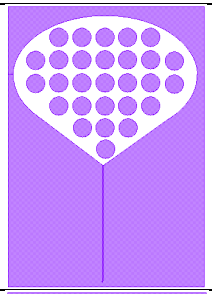	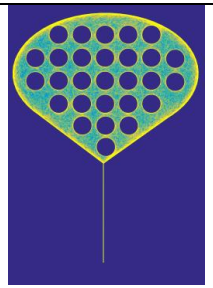				
Drop1_1	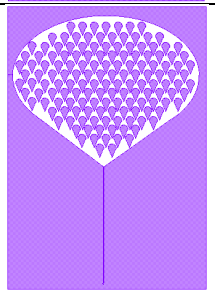	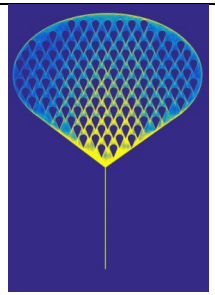	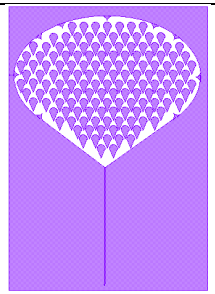	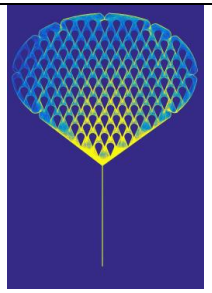	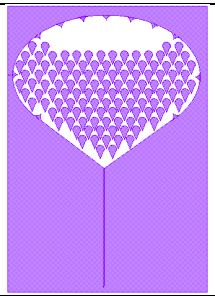	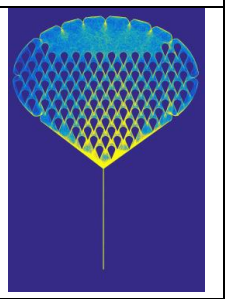
Drop1_2	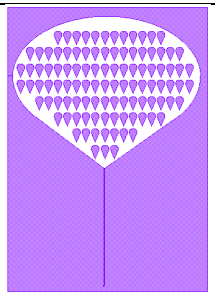	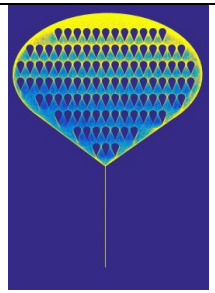	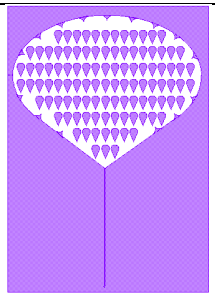	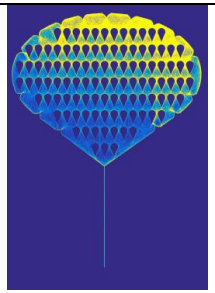		

	ZONE 1	ZONE 1	ZONE 2	ZONE 2	ZONE 3	ZONE 3
Figure1	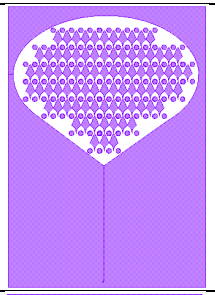	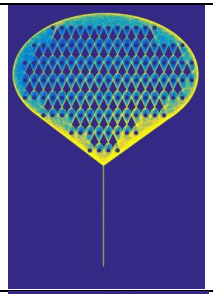			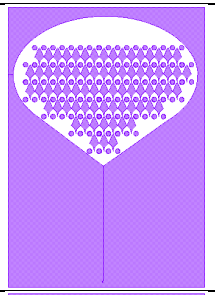	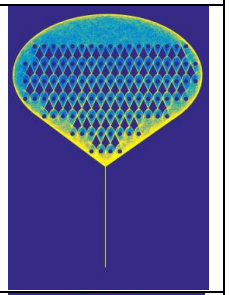
Figure 2	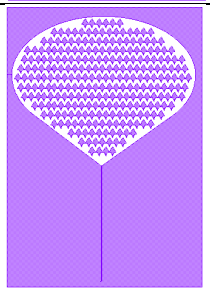	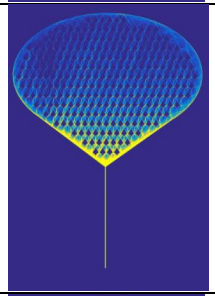	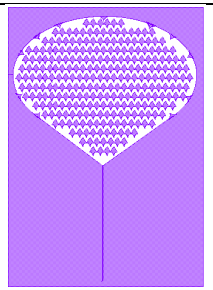		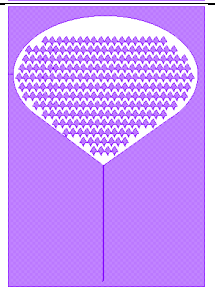	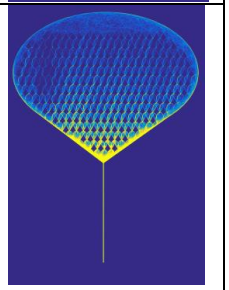
Flower 1	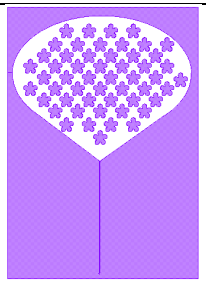	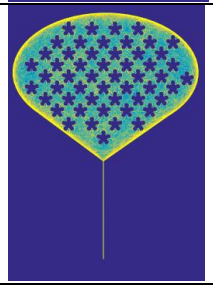	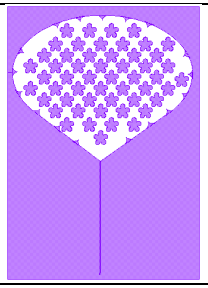	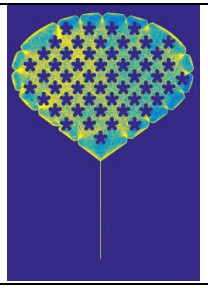		

	ZONE 1	ZONE 1	ZONE 2	ZONE 2	ZONE 3	ZONE 3
Flower 2	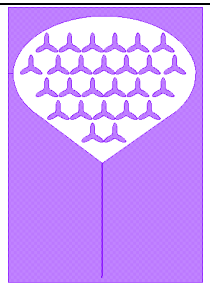	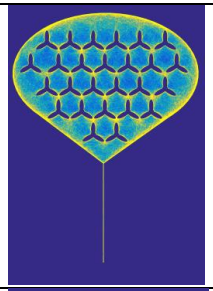	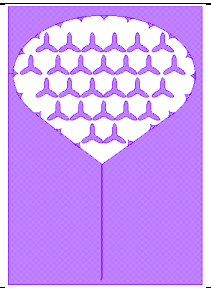	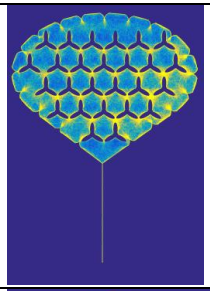		
Moon 1	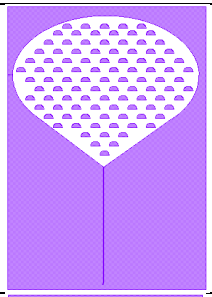	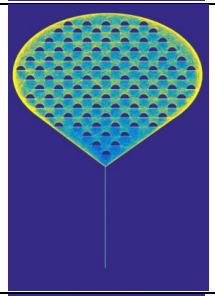	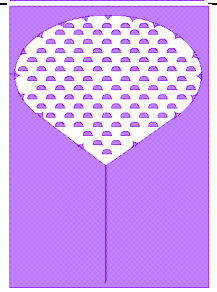	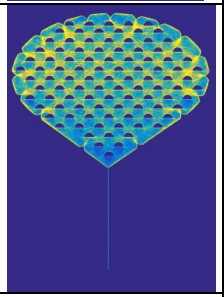		
Moon 2_1	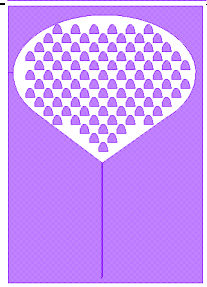	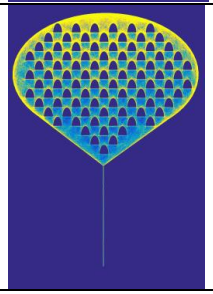				

	ZONE 1	ZONE 1	ZONE 2	ZONE 2	ZONE 3	ZONE 3
Moon 2_2	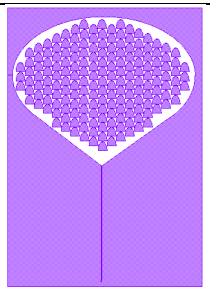	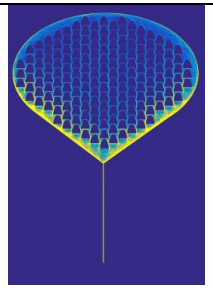			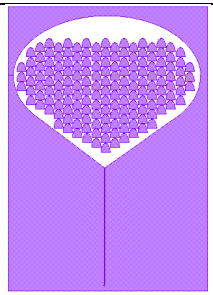	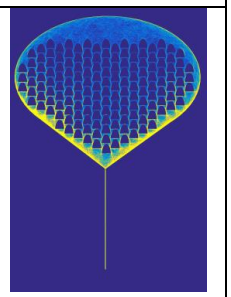
Triangle 1_1	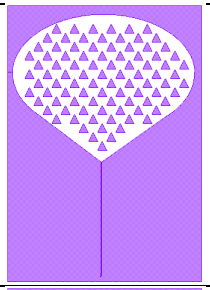	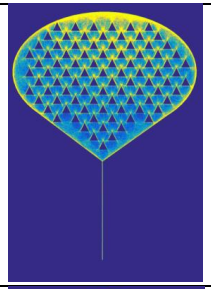	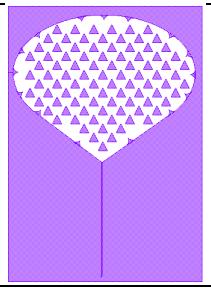	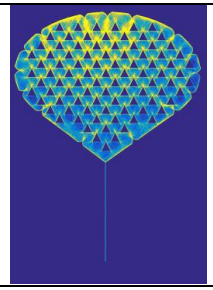	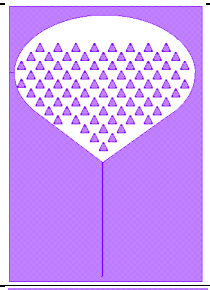	
Triangle 1_2	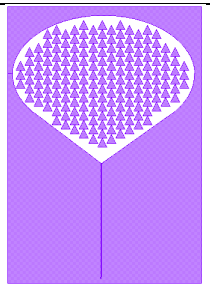	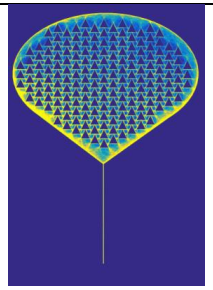			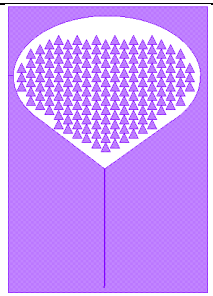	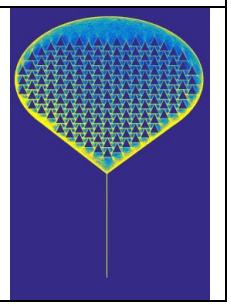

	ZONE 1	ZONE 1	ZONE 2	ZONE 2	ZONE 3	ZONE 3
Triangle 2_1	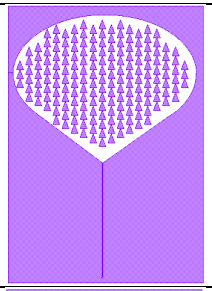	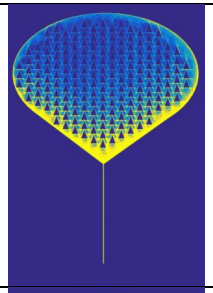			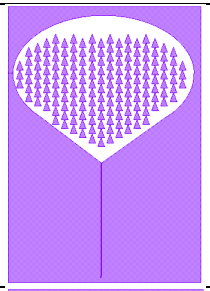	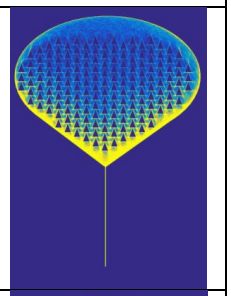
Triangle 2_2	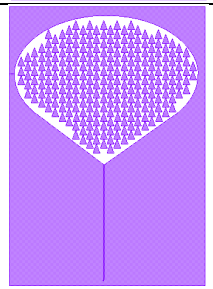	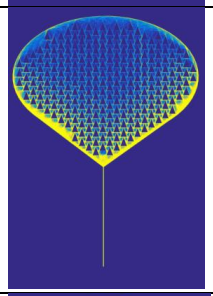			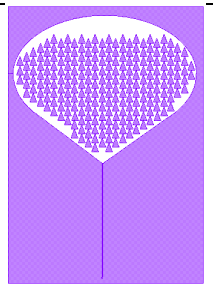	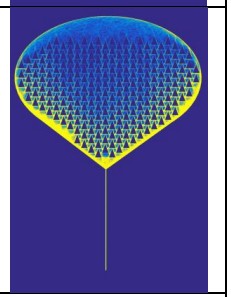
Triangle 3_1	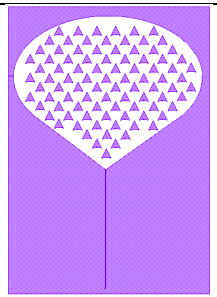	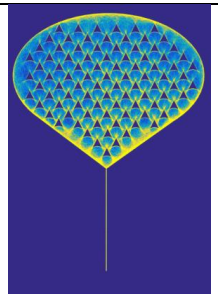	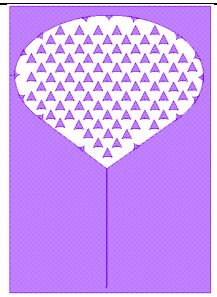	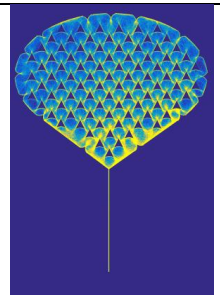		

	ZONE 1	ZONE 1	ZONE 2	ZONE 2	ZONE 3	ZONE 3
Triangle 3_2	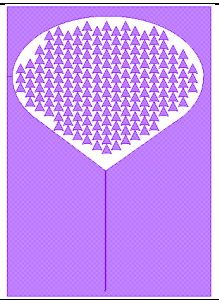	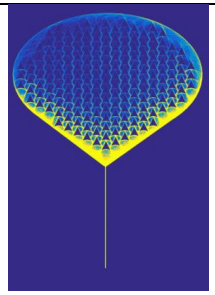	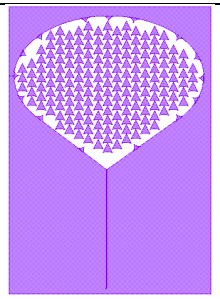	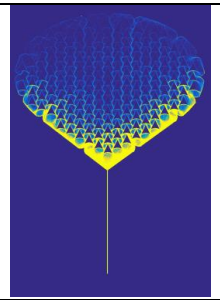	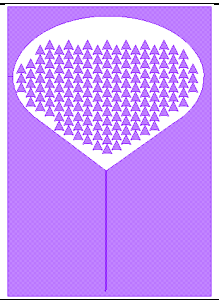	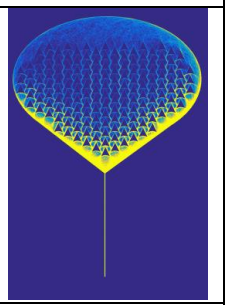
Triangle 4	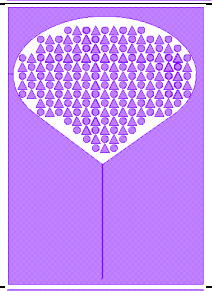	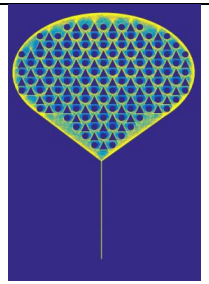	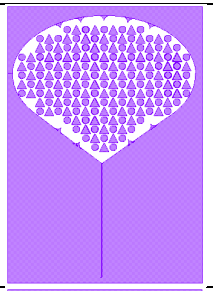	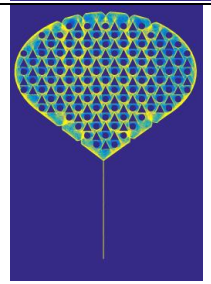		
Triangle 5	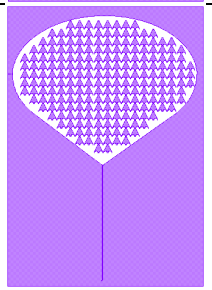	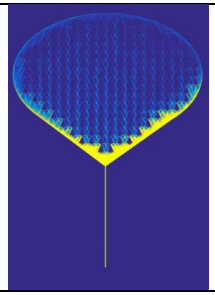	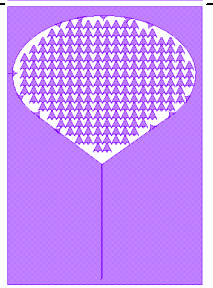	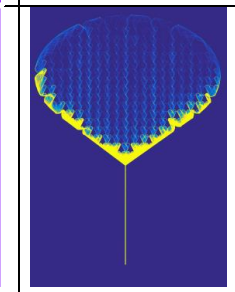	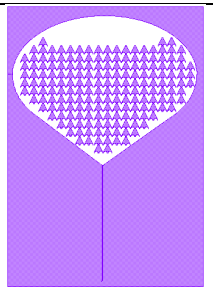	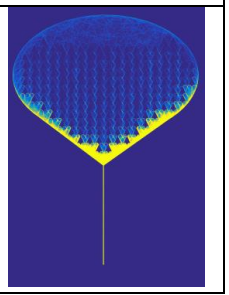

	ZONE 1	ZONE 1	ZONE 2	ZONE 2	ZONE 3	ZONE 3
Triangle 6_1	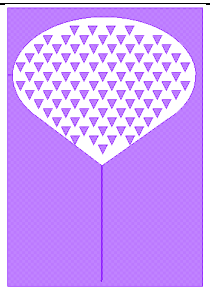	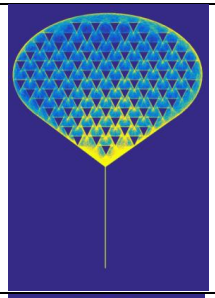	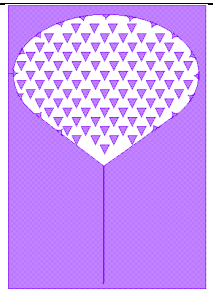	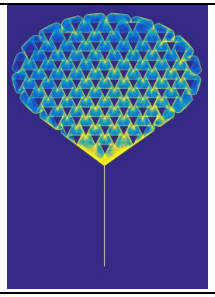		
Triangle 6_2	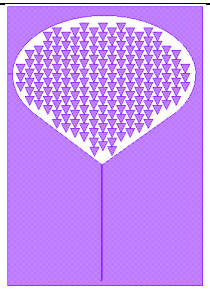	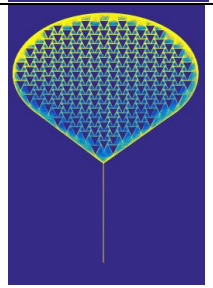			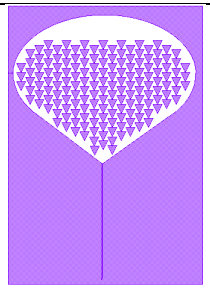	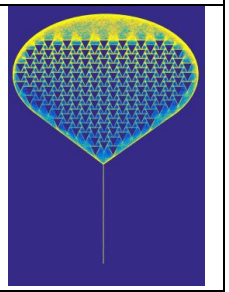
Triangle 7_1	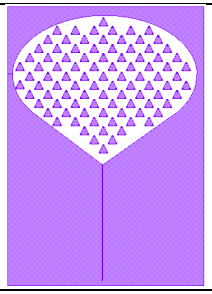	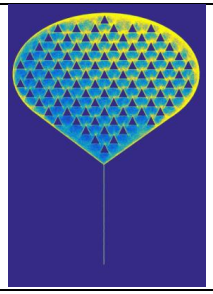	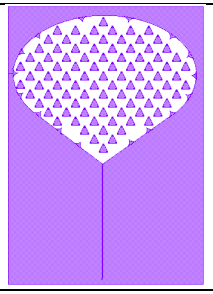	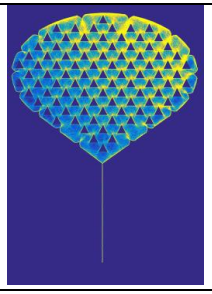		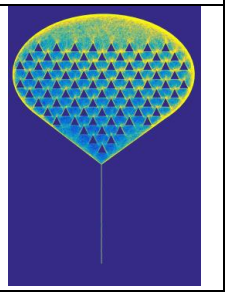

	ZONE 1	ZONE 1	ZONE 2	ZONE 2	ZONE 3	ZONE 3
Triangle 7_2